Thermodynamic properties of cis-1-chloro-2,3,3,3-tetrafluoro-1-propene [R-1224yd(Z)]: Experimental measurements of the density and speed of sound and modeling with the

International Journal of Refrigeration 155 (2023) 154–162

Contents lists available at ScienceDirect

International Journal of Refrigeration

journal homepage: www.elsevier.com/locate/ijrefrig

Thermodynamic properties of *cis*-1-chloro-2,3,3,3-tetrafluoro-1-propene [R-1224yd(Z)]: Experimental measurements of the density and speed of sound and modeling with the Patel–Teja equation of state

Propriétés thermodynamiques du cis-1-chloro-2,3,3,3-tetrafluoro-1-propène [R-1224yd(Z)] - Mesures expérimentales de la densité et de la vitesse du son et modélisation avec l'équation d'état de Patel-Teja

S. Lago [a,*], P.A. Giuliano Albo [a], R. Akasaka [b], R. Romeo [a]

[a] *Istituto Nazionale di Ricerca Metrologica, Strada delle Cacce 91, 10135, Italy*
[b] *Kyushu Sangyo University, 3-1 Matsukadai 2-chome, Higashi-ku, Fukuoka 813-8503, Japan*

ARTICLE INFO

Keywords:
R-1224yd(Z)
Density
Speed of sound
Equation of state
Cubic equation

Mots clés:
R-1224yd(Z)
Masse volumique
Vitesse du son
Équation d'état
Équation cubique

ABSTRACT

Measurements of compressed liquid density and speed of sound have been performed in *cis*-1-chloro-2,3,3,3-tetrafluoro-1-propene, also known as R-1224yd(Z). Density has been measured in the temperature range from 273.15 K to 353.15 K and for pressure up to 35 MPa. The relative expanded uncertainty ($k = 2$) for the obtained results has been estimated to be better than 0.05%. Speed of sound has been measured in the temperature range from 263 K to 353 K and for pressure up to 35 MPa. The expanded relative uncertainty ($k = 2$) for these measurements has been estimated to be better than 0.06%. Using the properties measured in this work and including measurements of vapor pressure and ideal gas specific heat capacity published in scientific literature, a Patel-Teja equation of state has been implemented for describing the properties of the refrigerant both in liquid and in vapor phase. An independent model for predicting the speed of sound has been proposed to allow to calculate the adiabatic compressibility of the fluid with an accuracy higher than that accessible from Patel-Teja formulation.

1. Introduction

R-1224yd(Z) (*cis*-1-chloro-2,3,3,3-tetrafluoro-1-propene, CAS No. 111512-60-8) is one of the environmentally friendly refrigerants suitable for large-scale centrifugal chillers and organic Rankine cycles, due to its non-flammability and preferable thermodynamic properties. The ozone depletion potential (ODP) and 100yr global warming potential (GWP) of R-1224yd(Z) are 0.00023 and 0.88, respectively (Tokuhashi et al., 2018), and the ANSI/ASHRAE safety classification (ANSI/ASHRAE Standard 34-2019, 2019) classifies R-1224yd(Z) into the safety group "A1" (no flame propagation and lower toxicity). The refrigeration industry considers this novel refrigerant as a promising alternative to 1,1,1,3,3-pentafluoropropane (R-245fa) or 2,2-dichloro-1,1,1-trifluoroethane (R-123). Some manufacturers have already launched centrifugal chillers that use R-1224yd(Z) as a refrigerant (Amano, 2019; Kanki and Maeda, 2020).

The first fundamental equation of state for R-1224yd(Z) was developed by Akasaka et al. (2017), which was often employed in analytical and/or experimental studies on this refrigerant, e.g., Mateu-Royo et al. (2019), Kujak et al., Giménez-Prades et al. (2022); however, the equation sometimes shows deviations larger than experimental uncertainties for recently published vapor pressures Sakoda and Higashi (2019), Beltramino et al. (2023) and liquid densities (Romeo et al., 2019; Fedele et al., 2020) because it is mainly based on limited and early experimental data (Fukushima et al.; Higashi and Akasaka, 2016) for the vapor pressure and (p, ρ, T) behavior. In addition, the first equation was not fitted liquid-phase speeds of sound; this may cause inaccurate predictions for the liquid enthalpy and heat capacities. For these reasons, it is necessary to improve the first equation with additional experimental data, including those for the liquid-phase speed of sound.

This work presents new experimental data for the density and speed of sound in the liquid phase. Currently, no data are available from the

* Corresponding author.
E-mail address: s.lago@inrim.it (S. Lago).

https://doi.org/10.1016/j.ijrefrig.2023.09.008
Received 26 April 2023; Received in revised form 24 July 2023; Accepted 11 September 2023
Available online 17 September 2023

Table 1
Information about the sample of R-1224yd(Z) measured.

Chemical name	CAS number	Source	Mass fraction purity %
cis-1-chloro-2,3,3,3- tetrafluoropropene	111512-60-8	AGC ltd.	> 99.25 %

public domain for the liquid-phase speed of sound of R-1224yd(Z). A vibrating tube densimeter was used for the density measurement and the double *pulse-echo* technique was applied to determine the speed of sound. In order to validate the thermodynamic consistency among the data obtained, they were correlated with the Patel-Teja (PT) equation of state (Patel and Teja, 1982). The correlation can be used to estimate the liquid properties of R-1224yd(Z) in engineering applications.

Generally, cubic equations of state such as the PT equation are intended to model volumetric properties at saturation state including vapor pressures and vapor–liquid equilibrium. Caloric properties such as heat capacities and speed of sound calculated from cubic equations are less accurate and often differ from experimental values by 20%. Akasaka et al. (2010) illustrated that deviations in isobaric heat capacities of R-1234yf calculated from the PT equation are always over 10% and sometimes exceed 25%. Gao et al. (2022) compared the isobaric heat capacities of R-1234yf and R-1234ze(E) calculated from the Peng-Robinson (PR) equation with the experimental data and confirmed that average deviations in calculated values are 4% to 6%; deviations become more significant for larger heat capacities. Ghoderao et al. (2023) reviewed the performances of 23 cubic equations of state in the prediction of the liquid isobaric heat capacity of various fluids and concluded that average deviations from experimental data are higher than 8% for all equations.

One reason for these observations is that fluid-specific parameters of the original PT equations are generalized for hydrocarbons. Actually, the PT equation provides reasonable predictions for the vapor-phase isobaric heat capacity and Joule-Thomson coefficient of methane; their typical deviations are 1.3% and 4.7%, respectively (Shoghl et al., 2021). If the parameters fitted to the fluid of interest are used, more reasonable values can be expected for the caloric properties. In this work, new adjustable parameters of the PT equation were introduced, which are determined by fitting the experimental data. This concept is similar to those of cubic equations with the volume translation, but the parameters introduced here are the ones dedicated to obtaining reasonable values both for the liquid density and liquid-phase speed of sound; no attempt has been ever made in this approach. Moreover, this approach could be applied to other cubic equations with slight modifications.

The following sections discuss the detail of experimental measurements, including the structure of the apparatuses, calibration methods, and uncertainty budgets. Information of the refrigerant sample used for the measurements is summarized in Table 1. The measured densities and speeds of sound are compared with values calculated from the first fundamental equation. Subsequently, the Patel-Teja equation of state fitted to the experimental data is presented, and deviations from experimental values are verified for the vapor pressure, density, speed of sound, and specific heat capacity. The conclusion mentions the review of the measurements and the outlook for developing a new fundamental equation.

2. Experimental measurements of density

Vibrating-tube densimeters are broadly used for measurements of density of liquid refrigerants, because of their high accuracy related to the operation simplicity. The vibrating tube densimeter consists of a glass or metallic U-shaped capillary tube, with a volume of a few cubic centimeters, placed in a thermostated cell. The measurement principle of vibrating-tube densimeters is based on the relation between the mechanical resonant frequency of the U tube, filled with the sample fluid, and the density of the fluid. The capillary is excited by a piezo-electric transducer coupled with the measurement cell and it vibrates

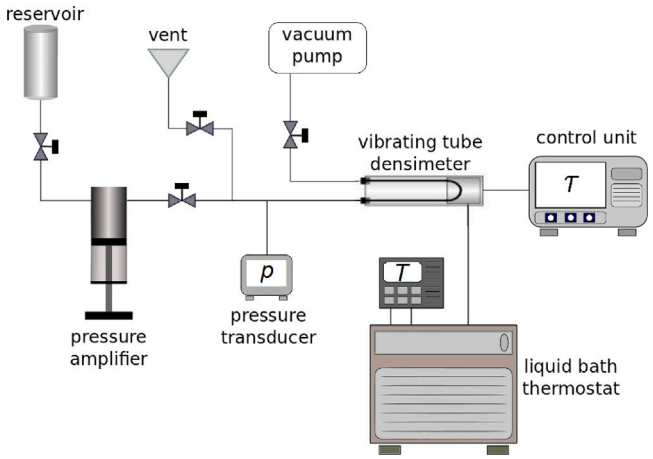

Fig. 1. Schematic representation of the experimental apparatus used to measure R-1224yd(Z) density.

perpendicular to its plane. The oscillation period, τ, corresponding to the value of a resonant frequency, is related to the value of the sample density, ρ, which depends mainly on the working temperature T and pressure p, by

$$\tau(T,p) = 2\pi\sqrt{\frac{M_0 + \rho V}{K(T,p)}}\ , \tag{1}$$

where K is the stiffness of the capillary, V is the tube inner volume and M_0 is the mass of the evacuated tube. The period of the harmonic oscillation of the tube can be directly related to the density, ρ, of the fluid contained in the tube by:

$$\rho(T,p) = A(T,p)\cdot\tau^2(T,p) - B(T,p)\quad , \tag{2}$$

where A and B, both temperature and pressure dependent, are characteristic parameters of the instrument, defined as

$$A = \frac{K(T,p)}{4\pi^2 V(T,p)}\quad ;\quad B = \frac{M_0}{V(T,p)}\quad , \tag{3}$$

The experimental apparatus for density measurements is schematically represented in Fig. 1. The core of the apparatus is an Anton Paar DMA 512P vibrating tube densimeter connected to a Anton Paar DMA 5000 used as counter unit and equipped with a high-pressure circuit used to fill and adjust the pressure inside the measuring capillary. The measurement cell, containing the vibrating tube, is also thermoregulated by a liquid bath thermostat and a platinum resistance thermometer PT100 is used to measure the temperature inside the densimeter, by means of a thermometer readout with an accuracy of 0.01 K. More details about the experimental apparatus can be found in Giuliano Albo et al. (2013).

2.1. Calibration procedure

In order to determine the instrument parameters the vibrating period in two reference fluids of known density has to be measured. However, to simplify the calibration procedure, the period is usually measured in the evacuated tube and, e.g., in water, for which Eq. (2) becomes, respectively:

$$0 = A(T,0)\cdot\tau_0^2(T,0) - B(T,0) \tag{4}$$

$$\rho_w(T,p) = A(T,p)\cdot\tau_w^2(T,p) - B(T,p) \tag{5}$$

However, there are many ways to analyze the results carried out by means of a vibrating tube densimeter. In several papers, the authors use different models to fit the experimental values or to calculate the density (Bouchot and Richon, 2001; Comuñas et al., 2008; Romeo et al., 2017). In particular, the approach proposed by Comuñas et al. (2008) assumes the hypothesis that the B parameter is both pressure and temperature dependent, while the A parameter only temperature dependent, and that it is valid the approximation $B(T,0) \simeq B(T,1\ \text{MPa})$. As a consequence, the unknown density can be obtained through the following relation

$$\rho(T,p) = \frac{\tau^2(T,p) - \tau_w^2(T,p)}{\tau_w^2(T,1\ \text{MPa}) - \tau_0^2(T)} \rho_w(T,1\ \text{MPa}) + \rho_w(T,p) \quad , \tag{6}$$

where ρ_w is the density of water and τ, τ_w, τ_0 are the measured periods related to the oscillation of the tube filled with the sample, with water and evacuated, respectively. Indeed, in this work, the calibration of the vibrating tube densimeter was performed by using as reference fluids water and vacuum. The oscillation period of pure water was measured in the temperature range of (273.15 and 343.15) K, along eight isotherms, and for pressure between (1 and 30) MPa, covering all the thermodynamic states where the refrigerants would be measured. The water densities used in the formula are the values provided by the reference equation of state of Wagner and Pruss (2002), which has a maximum relative standard uncertainty 0.003% in the studied T-p range.

The experimental densities presented in this paper were calculated through Eq. (6).

2.2. Uncertainty budget

In order to estimate its uncertainty, density was considered as a function of pure water density ρ_w, vibrating periods τ, τ_w, τ_0, temperature T and pressure p:

$$\rho = \rho(\rho_w, \tau, \tau_w, \tau_0, T, p) \ . \tag{7}$$

Applying the uncertainty propagation formula the relative uncertainty of density was estimated by

$$\frac{u(\rho)}{\rho} = \frac{1}{\rho}\left[\left(\frac{\partial\rho}{\partial\rho_w}\right)^{2u^2}(\rho_w) + \left(\frac{\partial\rho}{\partial\tau}\right)^{2u^2}(\tau) + \left(\frac{\partial\rho}{\partial\tau_w}\right)^{2u^2}(\tau_w) + \left(\frac{\partial\rho}{\partial\tau_0}\right)^{2} u^2(\tau_0) + \left(\frac{\partial\rho}{\partial T}\right)^{2u^2}(T) + \left(\frac{\partial\rho}{\partial p}\right)^{2u^2}(p)\right]^{1/2} . \tag{8}$$

The uncertainty of the reference water density is stated in Wagner and Pruss (2002). For vibrating period the uncertainty $u(\tau)$ is 0.1 μs corresponding to the repeatability of at least ten readings at each measuring point. The uncertainty of the PT100 resistance thermometer, $u(T)$, affecting the temperature measurement, is due to the fit calibration, the resolution of the instrument and the reading repeatability, and its value is 0.03 K. The pressure transducer expanded uncertainty $u(p)$ is 0.03 MPa, considering the uncertainty of the calibration and repeatability. The relative expanded uncertainty of density is calculated by applying the uncertainty propagation formula and it is 0.05% at the confidence level of 95%. In Table 2, all the sources and the associated uncertainties contributing to the density uncertainty are presented. It can be observed that the major contribution to the density uncertainty is due to the vibrating period measurements.

3. R-1224yd(Z) experimental results of density

The density of compressed liquid R-1224yd(Z) was measured along nine isotherms between 273.15 K and 353.15 K, with step of 10 K at pressures from (1 to 35) MPa. Table 3 contains the experimental densities at each measured temperature and pressure, which are reported in Fig. 2 as a function of pressure along isotherms. The experimental results were compared to the fundamental equation of state developed by Akasaka et al. (2017). In Fig. 3 the deviations of the experimental values from the equation of state (zero line) as a function of pressure are reported. All the measurements spread from the equation within 0.1%. Results were also compared to the literature measurements of Fedele et al. (2020). Fig. 4 shows that all the deviations are within ±0.2%, and most of them are within 0.1%, with very good agreement at the lower pressures.

Table 2
List of the uncertainty sources for the calculation of the combined expanded uncertainty (with k = 2) of density.

Uncertainty source		Relative magnitude %
water density	$\frac{\partial\rho}{\partial\rho_w}\frac{u(\rho_w)}{\rho}$	0.002
oscillation period	$\frac{\partial\rho}{\partial\tau}\frac{u(\tau)}{\rho}$	0.040
temperature	$\frac{\partial\rho}{\partial T}\frac{u(T)}{\rho}$	0.014
pressure	$\frac{\partial\rho}{\partial p}\frac{u(p)}{\rho}$	0.012
Relative expanded uncertainty (k=2)		**0.044**

Table 3
Experimental values of density in R-1224yd(Z). The overall expanded uncertainty is estimated to be 0.044% (k=2). The uncertainty of temperature, T, is 30 mK and 0.03 MPa for pressure, p.

T/K	p/MPa	ρ/kg m^{-3}	T/K	p/MPa	ρ/kg m^{-3}
273.157	1.187	1430.956	323.149	1.006	1291.043
273.154	4.992	1440.826	323.125	4.941	1309.707
273.162	10.008	1452.972	323.156	10.003	1330.327
273.155	14.944	1464.104	323.157	14.996	1348.061
273.180	20.044	1474.694	323.149	20.007	1364.049
273.164	25.103	1484.781	323.137	25.003	1378.429
273.165	29.962	1493.765	323.153	30.057	1391.457
273.163	35.219	1503.084	323.159	35.056	1403.670
283.160	1.118	1405.030	333.152	0.998	1259.490
283.171	5.008	1416.405	333.155	5.004	1281.262
283.149	10.147	1430.072	333.15	9.995	1304.118
283.143	15.006	1442.054	333.154	16.319	1328.478
283.142	19.989	1453.439	333.153	20.006	1341.138
283.135	25.001	1464.041	333.155	25.003	1356.733
283.154	29.989	1473.904	333.153	30.009	1370.977
283.302	34.988	1483.076	333.149	34.998	1384.039
293.151	1.004	1377.914	343.155	1.005	1226.137
293.153	5.006	1390.953	343.149	5.013	1251.615
293.147	10.006	1405.654	343.162	9.995	1277.503
293.146	14.999	1418.980	343.144	13.577	1293.415
293.151	20.007	1431.239	343.144	15.040	1299.423
293.155	24.992	1442.556	343.151	19.996	1318.297
293.150	30.005	1453.236	343.156	25.067	1335.194
293.154	34.982	1463.296	343.147	30.180	1350.588
			343.147	35.147	1364.413
303.151	1.006	1350.446	353.145	1.005	1190.439
303.151	5.004	1365.073	353.143	5.008	1220.533
303.151	10.004	1381.420	353.151	9.998	1249.904
303.151	10.009	1381.421	353.151	14.997	1274.084
303.153	15.002	1396.087	353.161	20.006	1294.805
303.154	15.006	1396.084	353.158	20.009	1294.818
303.149	20.001	1409.455	353.154	25.008	1313.077
303.152	20.002	1409.467	353.152	30.006	1329.562
303.152	25.005	1421.776	353.166	34.992	1344.471
303.149	30.005	1433.218	353.140	34.998	1344.514
303.160	30.007	1433.207			
303.155	35.005	1443.963			
313.161	0.991	1321.148			
313.162	5.008	1337.825			
313.148	9.989	1356.154			
313.151	15.004	1372.298			
313.221	20.020	1386.607			
313.198	25.019	1400.012			
313.135	30.000	1412.391			
313.160	30.005	1412.384			
313.153	35.019	1423.872			

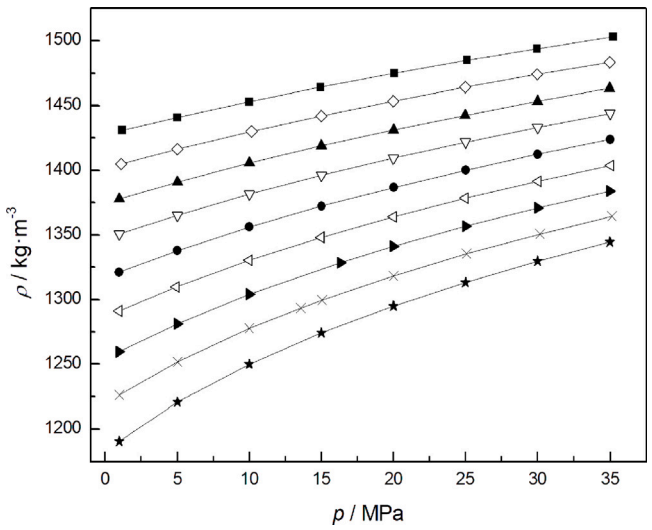

Fig. 2. R-1224y(Z) compressed liquid densities as a function of pressure: (■), T = 273.15 K; (◇), T = 283.15 K; (▽), T = 293.15 K; (•), T = 303.15 K; (◁), T = 313.15 K; (▶), T = 333.15 K; (×), T = 343.15 K, (★), T = 353.15 K.

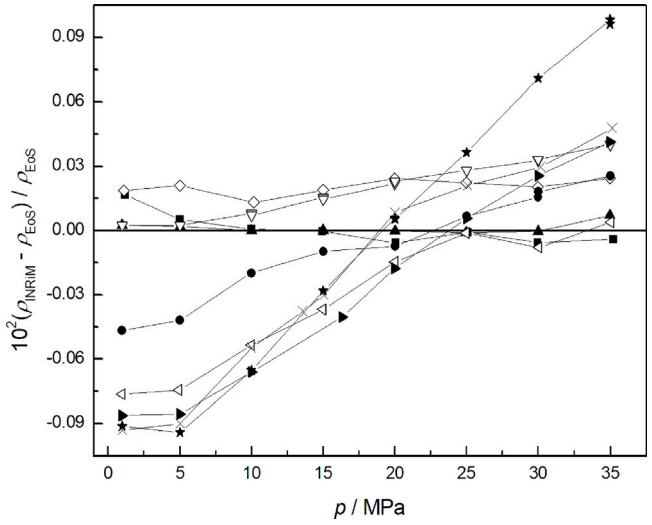

Fig. 3. Deviations of R-1224yd(Z) experimental densities from the fundamental equation of state of Akasaka et al. (2017) as a function of pressure: (■), T = 273.15 K; (◇), T = 283.15 K; (▽), T = 293.15 K; (•), T = 303.15 K; (◁), T = 313.15 K; (▶), T = 333.15 K; (×), T = 343.15 K, (★), T = 353.15 K.

4. Speed of sound experimental technique and apparatus

In this work, speed of sound measurements of a test sample of R-1224yd(Z) are presented in a temperature range between (263 and 353) K and for pressures up to 35 MPa. These measurements were carried out using an apparatus, which is detailed in previous works (Lago et al., 2006; Benedetto, 2005), specifically designed for the time of flight determination using the double *pulse-echo* technique. This experimental technique is suitable for accurate measurements of speed of sound over a wide range of temperature and pressure and is explained in detail in Trusler (1991). Indeed, this transient technique is an experimental method which has been widely used for the speed of sound measurements of a variety of fluids (Kortbeek et al., 1985; Ball and Trusler, 2001; Goodwin et al., 2003), including refrigerants (Lago S. Giuliano Albo et al., 2018).

With regard to the apparatus used in this work, a measuring cell consisting of two spacers, which are 45 mm (L_1) and 67.5 mm (L_2) long respectively, was used. The determination of these lengths was obtained by calibrating the ultrasonic cell over the temperature range involved in the experiment and at atmospheric pressure, using pure water as a reference fluid and using the IAPWS-95 (Wagner and Pruss, 2002) equation of state, for the determination of the speed of sound, w_w. Although they differ, depending on the thermodynamic conditions involved during the measurements, the temperature and pressure conditions used during the cell calibration are reported as (T_0, p_0), for reasons of better understanding and readability.

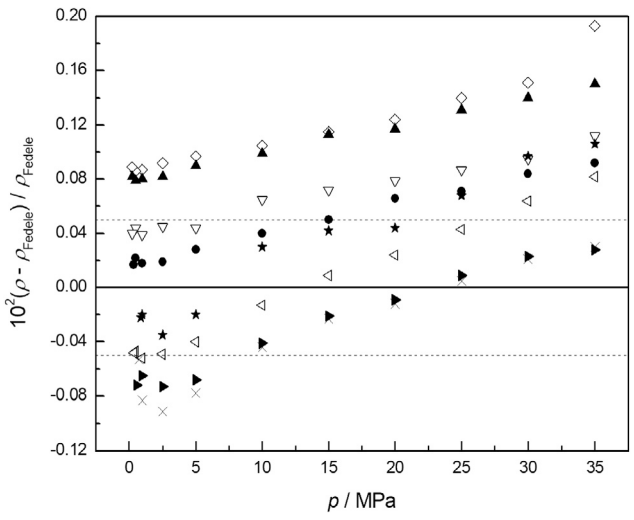

Fig. 4. Deviations of R-1224yd(Z) experimental densities from the measurements carried out by Fedele et al. (2020) as a function of pressure: (◇), T = 283.15 K; (▽), T = 293.15 K; (•), T = 303.15 K; (◁), T = 313.15 K; (▶), T = 333.15 K; (×), T = 343.15 K, (★), T = 353.15 K; - - -, maximum relative expanded uncertainty of Fedele et al. (2020) densities.

The working principle of the double *pulse-echo* technique is based on the measurement of the time of flight, τ, of two acoustic tone bursts spreading inside the sample fluid, as well as the length difference $\Delta L = L_2 - L_1$, which is the difference between the length L_1, namely the shorter cell spacer and the length L_2, that is the longer one. A piezoelectric ultrasonic transducer, which works both as an emitter and receiver, is placed inside of it and immersed in the fluid sample. A function generator excites the piezoelectric disc (which has an active diameter of 7 mm) at the resonance frequency of 4 MHz, with a sinusoidal five cycles tone-burst with a peak-to-peak amplitude of 10 V_{pp}. As a result of this, an ultrasonic wave spreads in opposite directions towards two steel reflectors located at the ends of the cell, at two different distances from the acoustic source. Thus, the echoes coming from the reflectors are sampled by a digital oscilloscope. The first echo $P_1(t)$, received by the piezoelectric disc after the time t, is correlated to the second echo $P_2(t+\tau)$, received at the time $t+\tau$, by a temporal correlation function $C(\tau)$. This function allows to accurately determine the time delay between the two echoes, τ_{exp}, as the value that maximizes $C(\tau)$.

$$C(\tau) = \int_{-\infty}^{+\infty} P_1(t) P_2(t+\tau) dt, \tag{9}$$

Then, it is possible to calculate the experimental speed of sound w_{exp} by determining the length $2\Delta L = 2(L_2 - L_1)$ and by measuring the time delay between the two echoes, as:

$$w_{exp} = \frac{2\Delta L}{\tau_{exp}}. \tag{10}$$

Since speed of sound measurements typically occur at temperatures and pressures significantly different from the conditions under which the cell is calibrated, (T_0, p_0), the acoustic path, ΔL, must be corrected to take into account the effects of thermal expansion and deformation due to high pressures. Eq. (11) represents this correction, where the

thermal expansion coefficient, α, and the compressibility coefficient, β_T, are those of the ultrasonic cell, made of AISI-316L stainless steel.

$$\Delta L(T,p) = \Delta L(T_0,p_0)\left(1+\alpha(T-T_0)-\frac{\beta_T}{3}(p-p_0)\right). \tag{11}$$

In addition, since the accuracy of the speed of sound measurement is highly dependent on the accuracy with which the time of flight could be measured, a further correction must be introduced that takes into account the diffraction effects due to the finite dimensions of the acoustic source used during the experiment. Thus, this correction must be applied to the term τ_{exp}, included in Eq. (10), and can be calculated using Eq. (12)

$$\delta t = \frac{\phi(2L_2)-\phi(2L_1)}{\omega_0}, \tag{12}$$

where ω_0 is the pulsation of the carrier wave, while $\phi(L_1)$ and $\phi(L_2)$ are the phase shifts related to a plane wave traveling the distances L_1 and L_2. These phase shifts are defined by the following integral form:

$$\phi(L) = Arg\left(1-\frac{4}{\pi}\int_{-\infty}^{+\infty} exp\left[-i\left(\frac{2\omega_0 b}{wL}\right)cos^2(\theta)\right]sin^2(\theta)d\theta\right), \tag{13}$$

where w is the speed of sound and b is the radius of the piezoelectric transducer. When the radius b of the transducer is much smaller than L, namely the spacers lengths, Eq. (13) can be rewritten in the following closed form Trusler (1991):

$$\phi(L) = \mathrm{Arg}\left[1-\exp\left(-\frac{iA}{2L}\right)\left(\mathrm{J}_0\left(\frac{A}{2L}\right)+i\mathrm{J}_1\left(\frac{A}{2L}\right)\right)\right], \tag{14}$$

where $A = 2\omega b^2/w_{exp}$, while J_0 and J_1 are Bessel functions of zero and first order, respectively. Expression (14) was used to determine the phase shift which occurs when an acoustic wave travels the distance L. Considering the dimensions involved in this experiment, the acoustic path traveled by the ultrasonic wave is more than ten times the radius of the acoustic source. Under these conditions, the correction for diffraction effects is estimated to be less than 0.0085% of the experimental value of τ.

In order to achieve the necessary stability at the required high pressures for speed of sound measurement, the ultrasonic cell is housed inside a stainless steel pressure vessel (AISI-316L). This pressure vessel is connected to a pressure amplifier which compresses the fluid, increasing its pressure up to 35 MPa. Finally, the system pressure is measured with a pressure transducer that has an uncertainty of 0.0004 MPa at ambient conditions and of 0.025 MPa for the highest pressure conditions.

The entire system consisting of pressure vessel, measuring cell and sample fluid is completely immersed inside the thermostatic bath, regulated by a Kambic thermostat (model: OB-30/2 ULT) which stabilizes the temperature to better than 0.01 K, as long as required to carry out an entire measurement. The temperature associated with the speed of sound is measured by taking the average of the temperatures measured by two platinum resistance thermometers (PT100), located on the upper and lower part of the pressure vessel. The resistance thermometers were calibrated against a 25 Ω standard platinum resistance thermometer (SPRT). Thanks to this configuration, it is possible to achieve a thermal gradient between the two PT100s between (10 and 60) mK, when the thermostatic bath is at thermal equilibrium. Finally, the calibration accuracy is estimated to be 0.02 K, which corresponds to the uncertainty associated to the temperature measurements. The experimental apparatus for speed of sound measurements is schematically represented in Fig. 5.

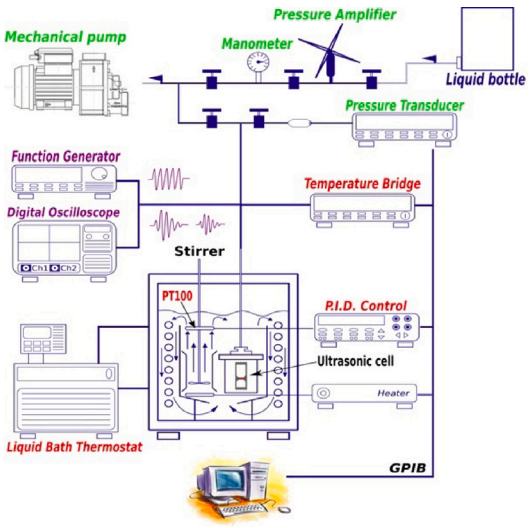

Fig. 5. Schematic representation of the experimental apparatus used to measure R-1224yd(Z) speed of sound.

4.1. Uncertainty budget

The basic principle of the double *pulse-echo* technique consists on measuring both the acoustic path, ΔL, and the time of fly, τ, an acoustic wave takes to cover the entire length inside the measuring cell. Then, after applying the corrections described above, it is possible to calculate the speed of sound, $w(T,p)$, at the measured T and p. The measurements uncertainty was estimated taking into account the different sources that contribute to its total balance. In this way, the estimated relative uncertainty can be calculated using the following equation for the propagation of the uncertainty:

$$\frac{u(w)}{w} = \sqrt{\left(\frac{u(\Delta L)}{\Delta L}\right)^2+\left(\frac{u(\tau)}{\tau}\right)^2+\left(\frac{u(T)}{w}\frac{\partial w}{\partial T}\right)^2+\left(\frac{u(p)}{w}\frac{\partial w}{\partial p}\right)^2+(R)^2}, \tag{15}$$

where R is the repeatability of the measurements.

The term $u(\Delta L)/\Delta L$, which appears within Eq. (15), represents the relative uncertainty associated with the determination of the acoustic path. Its value is obtained during the cell calibration, using as reference value the speed of sound of water given by the IAPWS-95 formulation (Wagner and Pruss, 2002), w_w, at room temperature, T_0, and atmospheric pressure, p_0. Thus, its uncertainty can be calculated, similarly to that of the speed of sound, as follows:

$$\frac{u(\Delta L)}{\Delta L} = \sqrt{\left(\frac{u(w_w)}{w_w}\right)^2+\left(\frac{u(\tau)}{\tau}\right)^2+\left(\frac{u(T_0)}{w_w}\frac{\partial w_w}{\partial T_0}\right)^2+\left(\frac{u(p_0)}{w_w}\frac{\partial w_w}{\partial p_0}\right)^2}. \tag{16}$$

Terms $u(T)$ and $u(p)$ are the expanded ($k = 2$) uncertainties associated to temperature and pressure measurements, respectively, considering instrument resolution, repeatability and instrument calibration. The sensitivity factors, $\partial w/\partial T$ and $\partial w/\partial p$, which appear in Eq. (15), were calculated from the experimental measurements of speed of sound, using polynomial interpolations at different T and p. The uncertainty associated with time of flight $u(\tau)$ is defined as double the oscilloscope sampling interval, which is $0.2 \cdot 10^{-9}$ s.

Table 4 shows the main uncertainty sources contributing to the calculation of the estimated uncertainty of speed of sound. Considering all these sources of uncertainties, the expanded overall relative uncertainty in speed of sound is estimated to be less than 0.06%, with a coverage factor k=2, over the entire region of measurements.

5. R-1224yd(Z) experimental results of speed of sound

During this work, speed of sound measurements were measured along nine isotherms, in a temperature range between (263.15 and 353.15) K. For each isotherm, it was chosen to start from the highest

Table 4
List of the uncertainty sources for the calculation of the overall uncertainty (with k = 2) of speed of sound.

Uncertainty source		Relative magnitude/%
Acoustic path length	$\frac{\partial w}{\partial \Delta L}\frac{u(\Delta L)}{w}$	0.020
Time of flight	$\frac{\partial w}{\partial \tau}\frac{u(\tau)}{w}$	0.002
Temperature	$\frac{\partial \tau}{\partial T}\frac{u(T)}{w}$	0.032
Pressure	$\frac{\partial w}{\partial p}\frac{u(p)}{w}$	0.037
Repeatability		0.017
Relative expanded uncertainty (k=2)		**0.055**

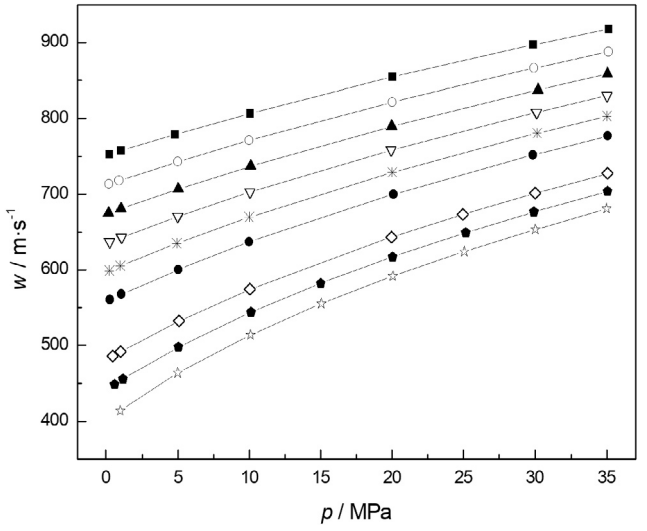

Fig. 6. Experimental values of speed of sound in R-1224yd(Z) along nine isotherms. (■) T = 263.15 K ; (○) T = 273.15 K ; (▲) T = 283.15 K ; (▽) T = 293.15 K; (✳) T = 313.15 K; (●) T = 323.15 K; (◇) T = 333.15 K; (⬟) T = 343.15 K; (☆) T = 353.15 K.

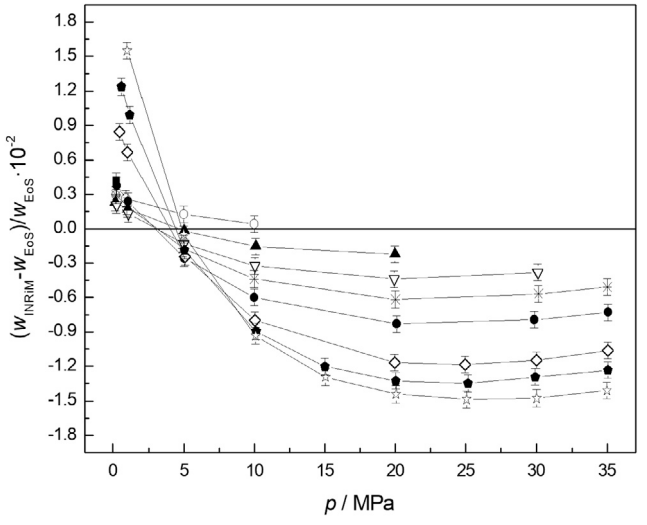

Fig. 7. Deviations of experimental speed of sound in R-1224yd(Z) from the expected values provided by the reference equation of state. (■) T=263.15 K ; (○) T=273.15 K ; (▲) T=283.15 K ; (▽) T=293.15 K; (✳) T=313.15 K; (●) T=323.15 K; (◇) T=333.15 K; (⬟) T=343.15 K; (☆) T=353.15 K.

pressure, p=35 MPa, gradually lowering it to atmospheric pressure or, in the case of higher temperatures, to the pressure where the signal-to-noise ratio was acceptable.

For each measurement cycle, pure sample was injected into a high pressure hydraulic line and inside the pressure vessel. System pressure was brought to the nominal measurement pressure by operating a pressure amplifier. Since the vapor pressure of R-1224yd(Z) is very close to the atmospheric pressure, the sample bottle was heated during the filling of the pressure vessel in order to increase the pressure of the system. In this way any vaporization of the refrigerant in the hydraulic line was avoided, keeping the fluid in a homogeneous liquid phase. Before starting a measurement on a new isotherm, the entire system consisting of pressure vessel, pressure amplifier and hydraulic line, was evacuated to prevent any contamination of the fluid during the refilling.

Table 5
Experimental values of speed of sound in R-1224yd(Z). The overall expanded uncertainty is estimated to be 0.055% (k=2). The uncertainty of temperature, T, is 10 mK and 0.01 MPa for pressure, p.

T/K	p/MPa	w/m s^{-1}	T/K	p/MPa	w/m s^{-1}
263.149	0.244	752.947	313.150	0.271	560.575
263.151	1.065	757.778	313.149	1.069	567.691
263.149	4.804	779.002	313.149	5.032	600.477
263.152	10.051	806.818	313.149	9.998	636.849
263.153	20.020	854.663	313.149	20.091	699.997
263.150	29.878	897.189	313.148	29.853	751.950
263.147	35.124	918.258	313.149	35.054	777.023
273.149	0.203	713.595	333.149	0.466	485.714
273.148	0.912	718.108	333.149	1.019	491.802
273.148	4.994	742.940	333.148	5.097	532.301
273.148	9.998	771.176	333.149	10.039	574.046
273.149	20.003	821.741	333.150	19.944	643.208
273.149	29.933	866.329	333.152	24.954	673.326
273.149	35.104	887.831	333.153	30.007	701.336
			333.150	35.042	727.464
283.149	0.174	674.712	343.141	0.598	448.400
283.149	1.044	680.685	343.150	1.186	455.678
283.150	5.027	706.691	343.149	5.036	497.675
283.150	10.100	737.089	343.149	10.122	544.087
283.150	19.965	789.680	343.149	14.999	582.205
283.151	30.213	837.660	343.148	20.036	617.106
283.154	35.043	858.511	343.149	25.157	649.128
			343.150	29.925	676.667
			343.151	35.041	703.869
293.150	0.251	636.836	353.149	1.002	414.170
293.149	1.087	643.063	353.149	4.993	463.543
293.150	4.992	670.550	353.150	10.089	513.996
293.149	10.036	702.835	353.152	15.051	555.244
293.150	19.924	758.449	353.152	20.047	591.546
293.151	30.098	808.203	353.150	25.054	624.124
293.154	35.012	830.247	353.151	30.020	653.510
			353.151	34.979	680.882
303.149	0.241	598.734			
303.148	1.006	604.963			
303.150	4.922	634.840			
303.151	9.987	669.528			
303.149	19.999	728.900			
303.150	30.152	780.670			
303.150	35.002	803.201			

Table 5 shows the experimental results of speed of sound in R-1224yd(Z), for temperatures ranging from (263 to 353) K and pressures up to 35 MPa, while in Fig. 6 they are plotted as a function of pressure.

Furthermore, Fig. 6 shows that speed of sound increases with pressure, while it decrease with respect to higher temperatures. It is also possible to see that the speed of sound is the more dependent on pressure, the higher the temperature and the lower the pressure.

The obtained experimental values were compared with those predicted by the reference equation of state for the thermodynamic properties of R-1224yd(Z) (Akasaka et al., 2017). This is a preliminary equation of state, which was developed without the contribution of any experimental speed of sound data. Therefore, performing this kind of measurements has a huge value in improving and redefining this model.

Then, Fig. 7 shows the deviations between the experimental measurements of speed of sound and the expected values, calculated using the equation of state.

Deviations at lower temperatures are limited to the lowest values of pressure, since the equation of state does not extend to high pressures for temperatures below 283.15 K. Instead, for higher temperatures, it is possible to compare the obtained results up to 35 MPa. The plot shows how the differences between experimental values and values predicted by the model have a similar trend for all isotherms. In fact, these have their maximum positive values at lower pressures while the maximum negative values are shown at higher pressures. The highest deviations occur at $T = 353.15$ K, where values above $\pm 1.5\%$ are reached at both higher and lower pressures. On the other hand, at $p = 5$ MPa, we have the minimum deviation values for all the isotherms, where they are all less than $\pm 0.3\%$.

6. Model for thermodynamic properties

For designing thermodynamic processes, a model based on experimental measurements is necessary. Among different possibilities, it was decided to propose a simple and widely used approach in chemical-engineering based on the Patel-Teja (PT) equation of state (Patel and Teja, 1982). With respect to Peng-Robinson cubic equation (PR), the PT model allows to fit the compression factor at the critical point that have the side effect of improving the predictions of vapor pressures. For modeling the thermal properties of the R-1224yd(Z) the following expression for the pressure as a function of temperature T and molar volume v was adopted:

$$p(T,v) = \frac{RT}{v-b} - \frac{a\alpha(T)}{v(v+b)+c(v-b)}\,, \tag{17}$$

where a, b and c are the parameters of the equation, R is the molar gas constant and

$$\alpha(T) = \left[1 + F\left(1 - \sqrt{\frac{T}{T_c}}\right)\right]^2 \tag{18}$$

is the Soave term with the adjustable parameter F while T_c is the critical temperature. Not all the parameters of expression (17) are independent, since the first and the second derivative, with respect to the volume, must be null at the critical point (T_c, v_c). This model requires that volumes are expressed in cubic meters per mole, temperatures in kelvin and pressures in pascal. Other derived quantities are calculated in terms of molar SI-units.

The formulation for specific heat capacities is obtained starting from ideal gas heat capacities $c_p^\circ(T)$ and $p(T,v)$ according to the following expressions:

$$c_v(T,v) = c_p^\circ(T) - R + T\int\left(\frac{\partial^2 p}{\partial T^2}\right)_v \mathrm{d}v\,, \tag{19}$$

$$c_p(T,v) = c_v(T,v) - T\left(\frac{\partial p}{\partial T}\right)^2\left(\frac{\partial v}{\partial p}\right)\,. \tag{20}$$

Usually the speed of sound $w(T,v)$ is then calculated as $w^2 = -(\gamma v^2/m)(\partial p/\partial v)_T$, where $\gamma = c_p/c_v$. However it was observed the obtained values can differ from experimental measurements up to 20% as shown, for example, by Akasaka et al. (2010). For this reason the following independent expression for speed of sound $w(T,v)$ is adopted:

$$w^2(T,v) = \frac{\gamma_0 v^2}{m}\left[\frac{RT}{(v-r)^2} - \frac{F_0\left[1 + F_1\left(1 - \sqrt{\frac{T}{T_c}}\right)\right]^2 (2v+q+r)}{[v(v+r)+q(v-r)]^2}\right]\,, \tag{21}$$

where m is the molar mass, γ_0, F_1, q and r are the fitting parameters and F_0 is determined so that $w^2(T_c, v_c) = 0$. In Table 6, the coefficients used to calculate thermal and caloric properties of R-1224yd(Z) are reported.

Table 6
Parameters for the expression (17), (18) and (21) used to predict thermal and caloric properties.

$T_c = 428.69$ K	$p_c = 3331$ kPa	$R = 8.31447$ J/(mol K)
$m = 148.4867 \cdot 10^{-3}$ kg/mol		
$a = 1.73658$	$b = 8.38329 \cdot 10^{-5}$	$c = 7.80204 \cdot 10^{-5}$
$F = 0.850394$	$\gamma_0 = 1.07422$	$F_0 = 0.424972$
$F_1 = 6.6206$	$r = 8.28852 \cdot 10^{-5}$	$q = -3.30939 \cdot 10^{-4}$

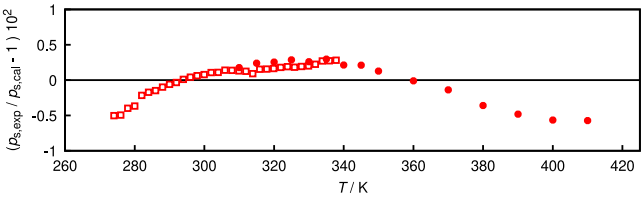

Fig. 8. Deviations of R-1224yd(Z) vapor pressures predictions $p_{s,\mathrm{cal}}$ from experimental results $p_{s,\mathrm{exp}}$ as a function of temperature: □ (Beltramino et al., 2023), • (Sakoda and Higashi, 2019), ○ (Bobbo et al., 2020).

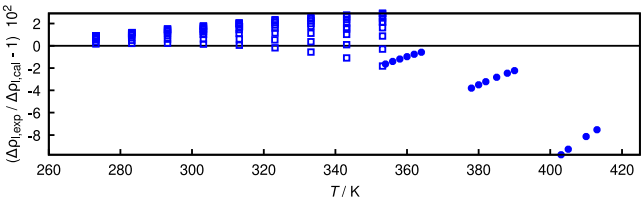

Fig. 9. Deviations of R-1224yd(Z) compressed liquid density predictions $\rho_{l,\mathrm{cal}}$ from experimental results $\rho_{l,\mathrm{exp}}$ as a function of temperature: □ this work, • (Sakoda and Higashi, 2019), ○ (Fedele et al., 2020).

7. Model predictions and discussion

Coefficients of the expression (17) have been obtained by the simultaneous fit to the vapor pressure by Beltramino et al. (2023), Sakoda and Higashi (2019) and Bobbo et al. (2020), together with the compressed liquid densities reported here. The comparison between the predictions for the vapor pressures and the corresponded experimental results are reported in Fig. 8, as a function of the temperature. The proposed model shows relative deviations better than 0.5% in the temperature range of 270 K and 410 K for the measurements of Beltramino et al. (2023) and Sakoda and Higashi (2019). The limited number of parameters for the equation does not allow to control the offset shown with the results of Bobbo et al. (2020), when compressed liquid densities are fitted together with vapor pressures.

In Fig. 9, predictions for the compressed liquid densities show deviations below 2% for temperature up to 370 K and pressure up to 35 MPa. Above 370 K (0.86 T_c), deviations increase up to 10% due to the limited accuracy of the here proposed model. It is known that the Soave form for $\alpha(T)$ is theoretically correct but unable to reproduce the thermodynamic behavior of fluids approaching the critical temperature. Alternative expressions can improve the predictions of the model; however, in this work, the simplicity of the formulation has been prioritized considering that without using extended formulations, the expected improvements are not significant.

Superheated vapor densities are also predicted with an accuracy in the order of 2% and the temperature dependence of the deviations is weaker respect to the one showed for compressed liquid densities, as reported in Fig. 10.

Caloric properties are usually estimated with a worse accuracy when simple models are adopted. For this reason, in this work, the speed of sound has not been calculated using the specific heat capacity ratio and isothermal compressibility but it has been represented using a separated form with its own parameters. Fig. 11 shows deviations of

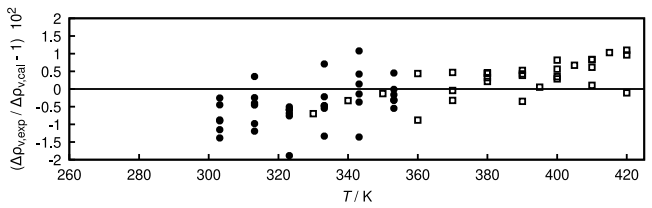

Fig. 10. Deviations of R-1224yd(Z) superheated vapor density predictions $\rho_{v,\mathrm{cal}}$ from experimental results $\rho_{v,\mathrm{exp}}$ as a function of temperature: □ (Sakoda and Higashi, 2019), • (Kano et al., 2020).

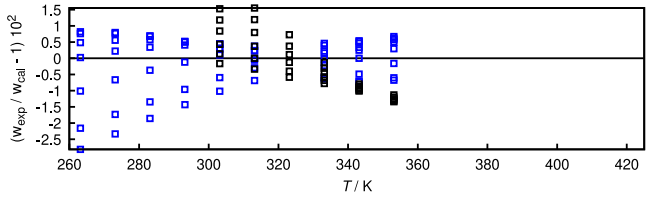

Fig. 11. Deviations of R-1224yd(Z) speed of sound predictions w_{cal} from experimental results w_{exp} as a function of temperature: □ this work (compressed liquid), • (Kano et al., 2020) (superheated vapor).

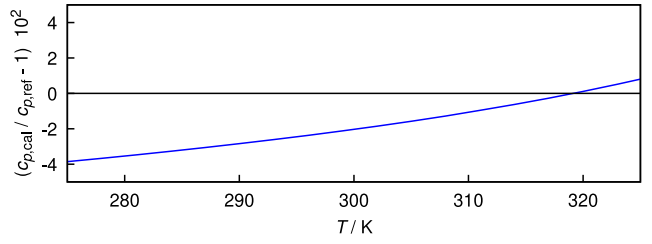

Fig. 12. Deviations of predicted R-1224yd(Z) isobaric specific heat capacity $c_{p,\mathrm{cal}}$ from those calculated using the linear fit reported in Fujiwara et al. (2016) $c_{p,\mathrm{ref}}$, as a function of temperature.

the experimental results in the order of 2% for the temperature range from (260 to 350) K and pressure up to 35 MPa.

Predictions for the specific heat capacities have been obtained using expressions (19) and (20) where the adopted form for isobaric ideal gas specific heat is the one reported in Kano et al. (2020). Authors are not aware of new published results in experimental measurements of specific heat capacities less than those of Fujiwara et al. (2016) obtained at 500 kPa and in the temperature range from 277 K to 325 K. Unfortunately, a table of measured values has not been included in the available paper, but estimations of c_p has been proposed in the form of the linear fit. Fig. 12 shows the deviations of the here implemented equation with respect to the values of specific heat capacity obtained from Fujiwara et al. (2016). In the considered temperature range of temperature the agreement is well within 5%.

8. Conclusion

Compressed liquid density and speed of sound of R-1224yd(Z) have been measured in a wide range of temperature and pressure, since available experimental measurements were insufficient to get an accurate formulation for the thermodynamic properties of this fluid. When available, the comparison of the results obtained in this work, with those published in scientific literature, confirmed to be in agreement within the estimated measurements uncertainty. When the results of this work are compared with those predicted by the preliminary equation of state of Akasaka et al. (2017), the deviations are in the order of 0.1% for compressed liquid density and of 1.7% for speed of sound. The disagreement suggested that a more accurate formulation of the equation of state could be obtained. The comparison supports the need of novel models and thus, a new fundamental equation of state for R-1224yd(Z) has been established based on the experimental data presented here and it will be published elsewhere (Akasaka and Lemmon, 2023). The experimental density and speed of sound obtained were also used to fit a Patel-Teja equation of state. The equation has been also analyzed comparing the model predictions with values of the vapor pressure, density, speed of sound, and specific heat capacity in the literature.

Declaration of competing interest

The authors declare that they have no known competing financial interests or personal relationships that could have appeared to influence the work reported in this paper.

References

Akasaka, R., Fukushima, M., Lemmon, E.W., 2017. A Helmholtz energy equation of state for cis-1-chloro-2, 3, 3, 3-tetrafluoropropene (R-1224yd(Z)). In: 21st European Conference on Thermophysical Properties, Graz, Austria, September 2017. pp. 3–8.

Akasaka, R., Lemmon, E.W., 2023. A Helmholtz energy equations of state for cis-1-chloro-2, 3, 3, 3-tetrafluoro-1-propene [R-1224yd(Z)]. Int. J. Thermophys (in press).

Akasaka, R., Tanaka, K., Higashi, Y., 2010. Thermodynamic property modeling for 2, 3, 3, 3-tetrafluoropropene (HFO-1234yf). Int J. Refrig. 33, 52–60.

Amano, S., 2019. High efficiency centrifugal chiller model RTBA using low GWP refrigerant R1224yd(Z). Ebara Eng. Rev. 257, 15–20.

ANSI/ASHRAE Standard 34-2019, 2019. Designation and safety classification of refrigerants.

Ball, S.J., Trusler, J.P.M., 2001. Speed of sound of n-hexane and n-hexadecane at temperatures between 298 and 373 k and pressures up to 100 MPa. Int. J. Thermophys. 22 (2), 427–443.

Beltramino, G., Rosso, L., Cuccaro, R., Fernicola, V., 2023. Saturation vapour pressure measurements of refrigerant R1224yd(Z) from 274 K to 338 K. Int. J. Refrig. 145, 90–95.

Benedetto, G., 2005. Speed of sound in pure water at temperatures between 274 and 394 K and at pressures up to 90 MPa. Int. J. Thermophys 26 (6), 1667–1680.

Bobbo, S., Bet, A., Scattolini, M., Fedele, L., 2020. Saturated pressure measurements of cis-1-chloro-2, 3, 3, 3- tetrafluoropropane (R1224yd (Z)) saturation pressure. J. Chem. Eng. Data 65, 4263–4267.

Bouchot, C., Richon, D., 2001. An enhanced method to calibrate vibrating tube densimeters. Fluid Phase Equilib. 191, 189–208.

Comuñas, M.J.P., Bazile, J.-P., Baylaucq, A., Boned, C., 2008. Density of diethyl adipate using a new vibrating tube densimeter from (293.15 to 403.15) K and up to 140 MPa, calibration and measurements. J. Chem. Eng. Data 53, 986–994.

Fedele, L., Bobbo, S., Scattolini, M., Zilio, C., Akasaka, R., 2020. HCFO refrigerant cis-1-chloro-2, 3, 3, 3 tetrafluoropropene [R1224yd(Z)]: Experimental assessment and correlation of the liquid density. Int. J. Refrig. 118, 139–145.

Fujiwara, N., Muto, Y., Sato, H., 2016. Measurement of heat capacity for refrigerant HCFO-1224yd(Z) by flow calorimeter. In: The Proceedings of the Symposium on Environmental Engineering, Vol. 26, no. 414. http://dx.doi.org/10.1299/jsmeenv.2016.26.414.

Fukushima, M., Hayamizu, H., Hashimoto, M., Thermodynamic properties of low-GWP refrigerant for centrifugal chiller. In: 16th International Refrigeration and Air Conditioning Conference at Purdue, West Lafayette, in, USA, July 2016. pp. 11–14.

Gao, N., Zhou, L., Wang, X., Chen, G., 2022. Evaluation of liquid heat capacity of latest low global warming hydrofluoroolefins (HFOs): A comparison of a cubic equation of state, fundamental equations of state, and a corresponding state equation. Int. J. Thermophys. 43 (9), 137.

Ghoderao, P.N., Narayan, M., Dalvi, V.H., Byun, H.S., 2023. Patel-Teja cubic equation of state–A review of modifications and applications till 2022. Fluid Phase Equilib. 567, 113707.

Giménez-Prades, P., Navarro-Esbrí, J., Arpagaus, C., Fernández-Moreno, A., Mota-Babiloni, A., 2022. Novel molecules as working fluids for refrigeration, heat pump and organic rankine cycle systems. Renew. Sust. Energ. Rev. 167, 112549.

Giuliano Albo, P.A., Lago, S., Romeo, R., Lorefice, S., 2013. High pressure density and speed-of-sound measurements in *n*-undecane and evidence of the effects of *near-field* diffraction. J. Chem. Thermodyn. 58, 95–100.

Goodwin, A., Marsh, K.N., Wakeham, W.A., 2003. Measurement of the thermodynamic properties of single phases. In: IUPAC Experimental Thermodynamics VI. pp. 435–451.

Higashi, Y., Akasaka, R., 2016. 11th Asian Thermophysical Properties Conference, Yokohama, Japan, October 2016. pp. 2–6.

Kanki, E., Maeda, M., 2020. Refrigeration unit and heat pump using low GWP refrigerant. Res. Dev. Kobe Steel Eng. Rep. 70 (1), 65–68.

Kano, Y., Kayukawa, Y., Fujita, Y., 2020. Dipole moment and heat capacity in the ideal gas state derived from relative permittivity and speed of sound measurements for HFO-1123 and HCFO-1224yd(Z). Int. J. Refrig. 118, 354–364.

Kortbeek, P.J., Muringer, M.J.P., Trappeniers, N.J., Biswas, S.N., 1985. Apparatus for sound velocity measurements in gases up to 10 kbar: Experimental data for argon. Rev. Sci. Instrum. 56 (1269).

Kujak, S., Schultz, K., Sorenson, E., Review of ultra-low GWP molecules–Thermodynamics properties and their characteristics for use in HVAC & R. In: IIR Rankine 2020 Conference–Advances in Cooling, Heating and Power Generation, Online, July 2020. pp. 27–31.

Lago, S., Giuliano Albo, P.A., Ripa, D.Madonna., 2006. Speed-of-sound measurements in n-nonane at temperatures between 293.15 and 393.15 K and at Pressures up to 100 MPa. Int. J. Thermophys. 27 (4), 1083–1094.

Lago S. Giuliano Albo, P.A., Brown, J.S., Bertinetti, M., 2018. High-pressure speed of sound measurements of trans-1-chloro-3, 3, 3-trifluoropropene (R-1233zd(E)) in liquid region for temperature from (273.15 to 353.15). K. J. Chem. Eng. Data 63 (11), 4039–4045.

Mateu-Royo, C., Navarro-Esbrí, J., Mota-Babiloni, A., Amat-Albuixech, M., Molés, F., 2019. Thermodynamic analysis of low GWP alternatives to HFC-245fa in high-temperature heat pumps: HCFO-1224yd(Z), [HCFO-1233zd(E) and HFO1336mzz(Z)]. Appl. Therm. Eng. 152, 762–777.

Patel, N., Teja, A., 1982. A new cubic equation of state for fluids and fluid mixtures. Chem. Eng. Sci. 37 (3), 463–473.

Romeo, R., Giuliano Albo, P.A., Lago, S., Brown, J.S., 2017. Experimental liquid densities of cis-1, 3, 3, 3-tetrafluoroprop-1-ene (R1234ze(Z)) and trans-1-chloro-3, 3, 3-trifluoropropene (R1233zd(E)). Int. J. Refrig. 79, 176–182.

Romeo, R., Lago, S., Giuliano Albo, P.A., 2019. Density measurements of compressed (Z)-1-chloro-2, 3, 3, 3, -tetrafluoropropane (HCFO-1224yd(Z)). In: 12th Asian Thermophysical Properties Conference, Xi'an, China, October 2019. pp. 2–6.

Sakoda, N., Higashi, Y., 2019. Measurements of PvT properties, vapor pressures, saturated densities, and critical parameters for cis-1-chloro-2, 3, 3, 3-tetrafluoropropane (R1224yd(Z)). J. Chem. Eng. Data 64, 3983–3987.

Shoghl, S.N., Naderifar, A., Farhadi, F., Pazuki, G., 2021. Comparing the predictive ability of two-and three-parameter cubic equations of state in calculating specific heat capacity, Joule-Thomson coefficient, inversion curve and outlet temperature from Joule-Thomson valve. Cryogenics 116, 103288.

Tokuhashi, K., Uchimaru, T., Takizawa, K., Kondo, S., 2018. Rate constants for the reactions of OH radical with the $(E)/(Z)$ isomers of $CF_3CF{=}CHCl$ and $CHF_2CF{=}CHCl$. J. Phys. Chem. A 122 (12), 3120–3127.

Trusler, J.P.M., 1991. Physical Acoustics and Metrology of Fluids. CRC Press.

Wagner, W., Pruss, A., 2002. The IAPWS formulation 1995 for the thermodynamic properties of ordinary water substance for general and scientific use. J. Phys. Chem. Ref. Data 31, 387–535.